Electronic Supplementary Information

Reduced Interfacial Tension on Ultrathin NiCr-LDH Nanosheets Arrays for Efficient Electrocatalytic Water Oxidation

Xiuxiu Zhang,[a] Xuan Sun,[a] Yuanli Li,[a,b] Fengchun Hu,[a]* Yanzhi Xu,[a] Jie Tian,[c] Hui Zhang,[a] Qinghua Liu,[a] Hui Su,[a]* and Shiqiang Wei[a]

[a] *National Synchrotron Radiation Laboratory, University of Science and Technology of China, Hefei 230029, Anhui, P. R. China*

[b] *Fundamental Science on Nuclear Wasters and Environmental Safety Laboratory, Southwest University of Science and Technology, Mianyang 621010, Sichuan, P. R. China*

[c] *Material Test and Analysis Lab, Energy and Materials Science Experiment Center, University of Science and Technology of China, Hefei 230026, Anhui, P. R. China*

*E-mail: fchu@ustc.edu.cn; suhui@ustc.edu.cn

Experimental details

Materials. $Ni(NO_3)_2 \cdot 6H_2O$, $Cr(NO_3)_3 \cdot 9H_2O$, urea, N,N-dimethylformamide (DMF), and absolute ethanol were purchased from Sinopharm Chemical Reagent Co., Ltd. Naphthalene-2,6-dicarboxylic acid (NDC) were purchased from Alfa Aesar. All chemicals were used directly without further purification. Deionized (DI) water was used in all experiments.

Synthesis of pristine NiCr-LDH nanosheets (NiCr-LDH). Ni foam (NF) was used as the substrate. Firstly, the NF was washed in an ultrasonic bath of acetone for 10 min. Subsequently, it soaked in diluted HCl solution (3.0 M) for 10 min to remove the surface oxidation layer, and then washed with absolute ethanol and deionized water for 10 min, successively. NiCr-LDH on NF was synthesized by hydrothermal method.[1] In a typical procedure, $Ni(NO_3)_2 \cdot 6H_2O$ (0.2617 g, 0.9 mmol), $Cr(NO_3)_3 \cdot 9H_2O$ (0.2401 g, 0.6 mmol), and urea (0.2402 g, 4 mmol) were dissolved in 36 mL DI water under stirring to form a clear solution. A piece of the cleaned NF (2 cm×2.8 cm) was immersed in a 50 mL Teflon-lined stainless steel autoclave with above mixture solution. The autoclave was sealed and maintained at 120℃ for 12 h. After cooling down to room temperature, the sample was obtained and rinsed with DI water 3 times and dried in a vacuum oven at 60 ℃ for 3 h.

Synthesis of ultrathin NiCr-LDH nanosheets arrays (NiCr-LDH NSAs). Typically, 80 mg of NDC was dissolved in mixed solution of DMF (15 mL) and DI water (1.5 mL). Subsequently, the above solution was transferred into a 50 mL Teflon-lined stainless steel autoclave, and then a piece of NiCr-LDH/NF was immersed into the reaction solution. The autoclave was sealed and maintained at 100℃ for 24 h. After cooling down to room temperature, the sample was obtained and rinsed with absolute ethanol and DI water 3 times and then dried in a vacuum oven at 60 ℃ for 3 h. The

mass loading of final ultrathin NiCr-LDH nanosheets arrays on NF was about 1.96 mg cm^{-2}.

Characterizations. The field emission scanning electron microscopy (SEM) images and energy dispersive X-ray spectroscopy (EDS) were taken on a Gemini SEM 500 scanning electron microscope. Transmission electron microscopy (TEM) images, high-resolution transmission electron microscopy (HRTEM) images and energy dispersive spectroscopy (EDS) were acquired on a JEM-2100F microscope with an acceleration voltage of 200 kV. Atomic force microscopy (AFM) images were performed by DI Multimode V Scanning Probe Microscope. The X-ray diffraction (XRD) patterns of samples were measured in a Philips X'Pert Pro Super X-ray diffractometer with Cu Kα radiation (λ = 1.54178 Å). The powder samples physically detached from NF were also used for the XRD testing to alleviate the influence of NF on the results. X-ray photoelectron spectroscopy (XPS) was recorded on a Thermo ESCALAB 250Xi with Al Kα (hν =1486.6 eV) as the excitation source. With reference to C 1s to 284.5 eV, the binding energy obtained in XPS spectra analysis was corrected. The wettability of samples was evaluated using a SDC-350 contact angle system with a droplet size of 2 μl. The images of water drops were snapped 15 s after the deposition of the drop on the samples. The Ni L-edge X-ray absorption near-edge spectra (XANES) were measured at BL12B-a beamline of NSRL in the total electron yield mode by collecting the sample drain current under a vacuum better than that at 5×10^{-8} Pa.

XAFS measurements and EXAFS fitting details. The Ni and Cr *K*-edge XAFS data were collected at the 1W1B station in Beijing Synchrotron Radiation Facility (BSRF, China). The storage rings of BSRF were operated at 2.5 GeV with a maximum current of 250 mA. To obtain the detailed structural parameters around Ni and Cr atoms in the samples, the EXAFS data were processed according to the standard procedures using

the ATHENA and ARTEMIS module implemented in the IFEFFIT software packages. In order to eliminate the influence of NF on the results, powder samples detached from NF were used for Ni *K*-edge testing. The amplitude reduction factor S_0^2 was also treated as adjustable variable and the obtained value of 0.90 for nickel foil was fixed in fitting the subsequent Ni *K*-edge data for samples. The fit was done on the k^3-weighted EXAFS function χ(k) data from 2.6 to 12.9 $Å^{-1}$ in the R-range of 1.0–3.3 Å. The samples on NF were directly used for Cr *K*-edge testing. The amplitude reduction factor S_0^2 was also treated as adjustable variable and the obtained value of 0.81 for chromium foil was fixed in fitting the subsequent Ni *K*-edge data for samples. The fit was done on the k^3-weighted EXAFS function χ(k) data from 2 to 11 $Å^{-1}$ in the R-range of 1.0–2.2 Å. The coordination numbers *N*, interatomic distances *R*, Debye-Waller factor σ^2 and the edge-energy shift ΔE_0 were allowed to run freely.

***Operando* SR-FTIR measurements.** *Operando* synchrotron radiation FTIR data were collected by a homemade top-plate cell reflection IR setup with a CaF_2 crystal as the infrared transmission window (cutoff energy of ~625 cm^{-1}) at the infrared beamline BL01B of the National Synchrotron Radiation Laboratory (NSRL, China). In order to reduce the loss of infrared light during in situ infrared testing, the catalyst electrode was tightly pressed against the CaF_2 crystal window with micron gaps. The apparatus adopted the reflection mode with vertically incident infrared light to ensure the quality of the SR-FTIR spectra. Each infrared absorption spectrum was acquired by averaging 514 scans at a resolution of 2 cm^{-1}. All infrared spectral acquisitions were carried out after a constant potential was applied to the catalyst electrode for 250 s. The background spectrum of the catalyst electrode was acquired at an open-circuit voltage before OER measurement, and the measured potential ranges were 1.2 - 1.7 V with an interval of 0.1 V.

Electrochemical Measurements. Electrochemical measurements of OER performance were performed using an electrochemical workstation (Model CHI760E, CH instruments, Inc., Austin, TX) with a standard three-electrode electrochemical cell, operated with the self-supporting array grown on NF (the active area of 1×1 cm^{-2}, mass loading ~1.96 mg cm^{-2}) as the working electrodes, carbon rode as the counter electrode, and the normal Hg/HgO electrode as the reference electrode. All final potentials was converted to reversible hydrogen electrode (RHE) with the conversion E (vs. RHE) = E (vs. Hg/HgO) + 0.098 V + 0.059 × PH. Linear sweep voltammetry (LSV) curves were obtained at a rate of 1 mV s^{-1} with IR correction after several cyclic voltammetry tests until stable. The electrochemical double-layer capacitance (C_{dl}) was calculated by cyclic voltammetry curves in the region of between 1.20 and 1.30 V vs. RHE with scanning rates of 2, 4, 6, 8, and 10 mV s^{-1}. The ECSA values were calculated from the measured double layer capacitance divided by the specific capacitance of an atomically smooth material: ECSA = C_{dl} / C_s. The measured potential ranges of the electrochemical impedance spectroscopy (EIS) were 1.450-1.800V (vs. RHE) in the frequency range of 0.01-100000 Hz. For comparison, 5 mg of NiCr-LDH NSs and RuO_2 powder were dispersed into a mixture solution of 30 μL of Nafion (5%, Sigma-Aldrich), 250 μL of ethanol, and 750 μL of distilled water ultrasonically to form homogeneous catalyst ink. Then, 404 μL of the resulting catalyst ink was coated on NF. All the tests were carried out in 1.0 M KOH solution.

It is assumed that every active metal atom of the catalyst participates in the reaction. The turnover frequency (TOF, s^{-1}) can be calculated according to the equation: TOF = ($j \times A$) / ($4 \times F \times M$), where j is the current density at a given potential, A is the surface of the electrode, F is the faradaic constant, and M is the number of moles of active metal on the electrode. The mass activity (A g_{Ni}^{-1}) can be calculated according to the equation: Mass activity = ($j \times A$) / m, where j is the current density at a given potential, A is the

surface of the electrode, and *m* is the active metal loading mass on the electrode. Previous experiments and DFT calculations of NiCr-LDH have confirmed that Ni is likely to be the effective active site and Cr acts as synergetic site for adjusting the electronic structure of Ni.[2-4] The loading mass of active metal components on the electrode is determined by the inductively coupled plasma mass spectrometry (ICP-MS) measurements (Table S5).

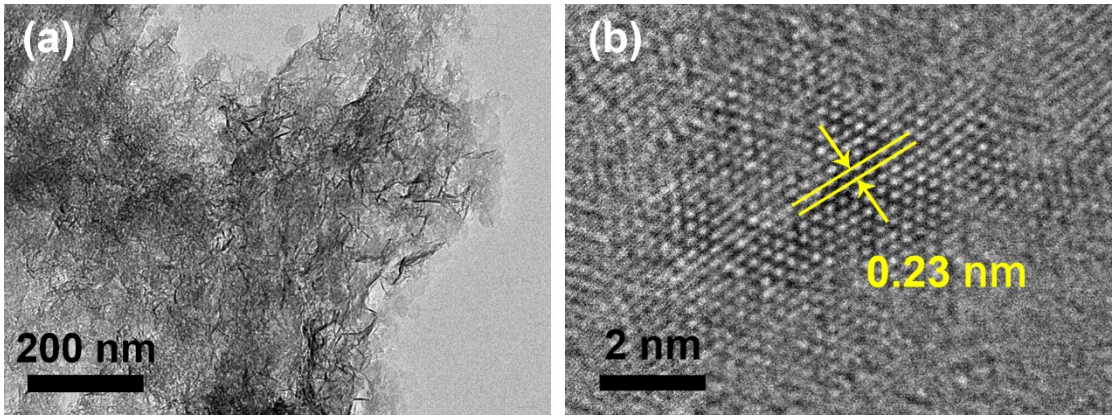

Figure S1. (a) TEM image and (b) HRTEM image of NiCr-LDH.

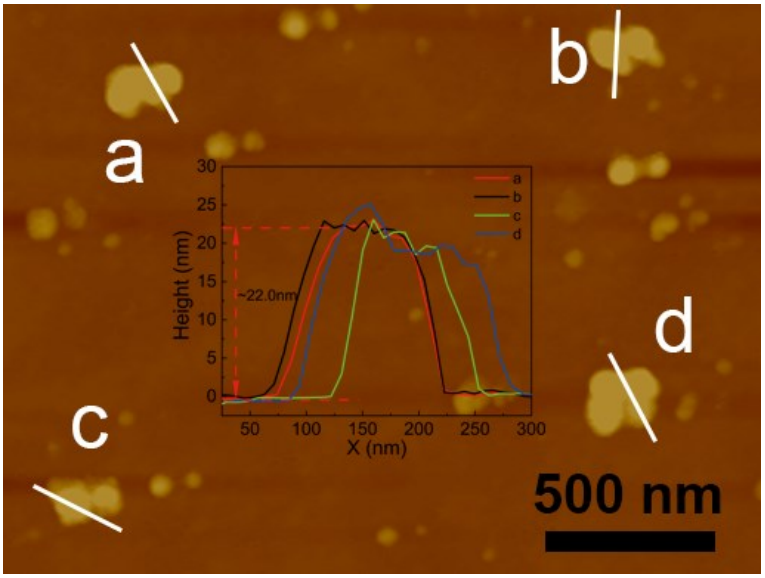

Figure S2. AFM image of NiCr-LDH and the corresponding height profile measured along the white line.

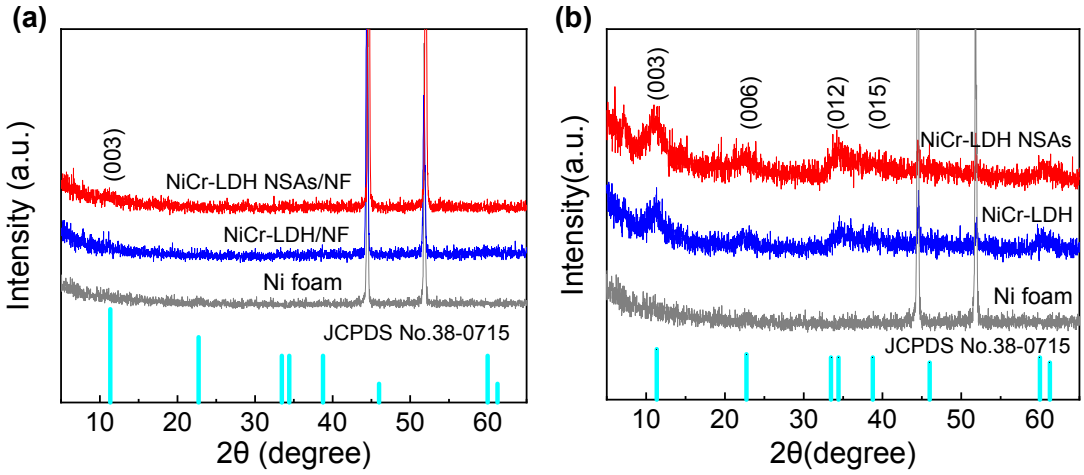

Figure S3. XRD patterns of (a) the samples on Ni foam and (b) the powder samples physically detached from Ni foam.

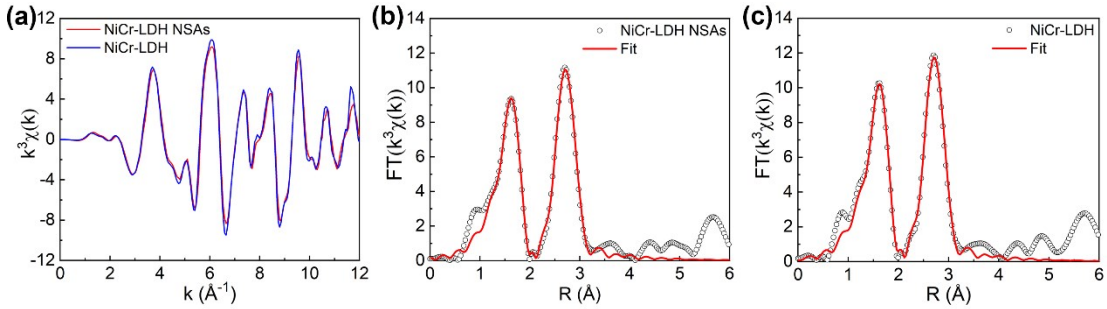

Figure S4. (a) The Ni *K*-edge EXAFS $k^3\chi(k)$ oscillation function and (b, c) the Ni *K*-edge EXAFS fitting results of NiCr-LDH NSAs and NiCr-LDH.

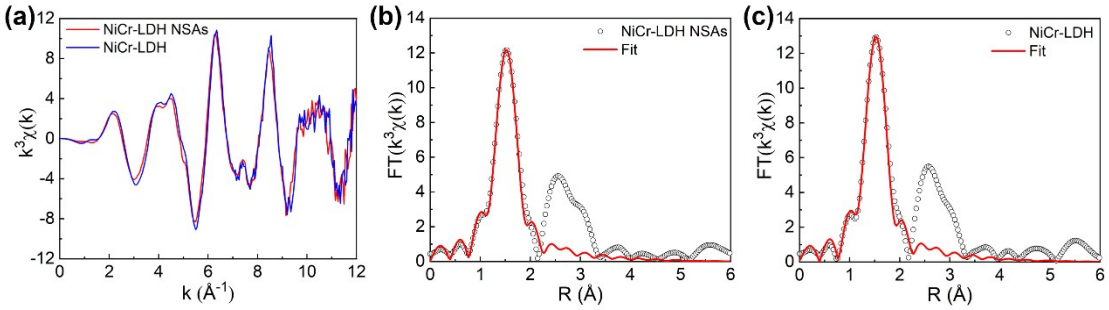

Figure S5. (a) The Cr *K*-edge EXAFS $k^3\chi(k)$ oscillation function and (b, c) Cr *K*-edge EXAFS fitting results of NiCr-LDH NSAs and NiCr-LDH.

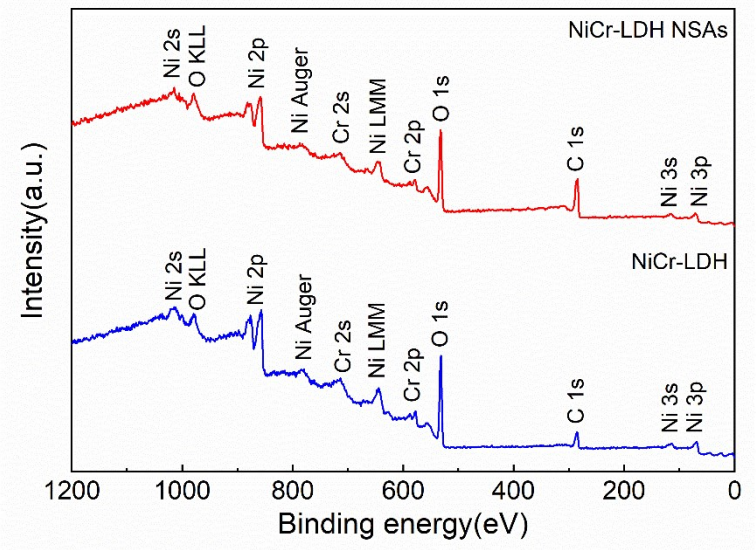

Figure S6. XPS results of NiCr-LDH NSAs and NiCr-LDH.

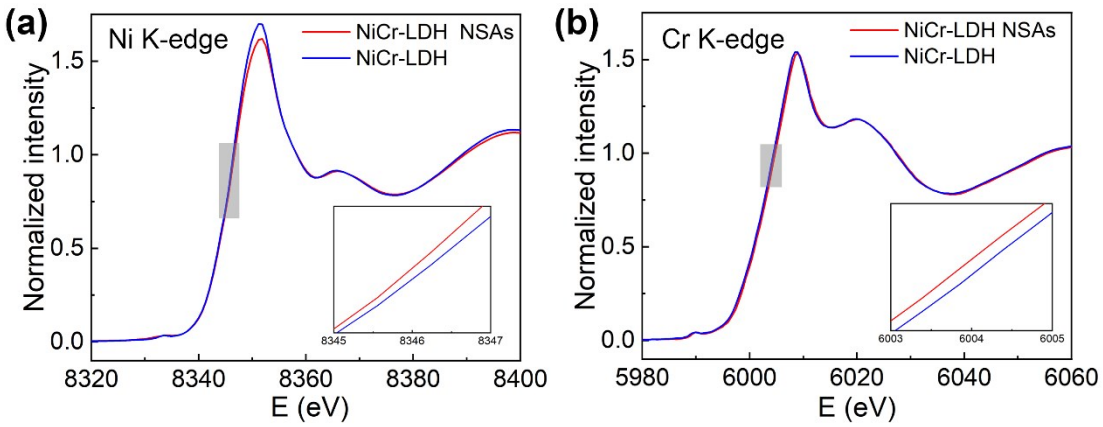

Figure S7. (a) Ni *K*-edge XANES spectra and (b) Cr *K*-edge XANES spectra of NiCr-LDH NSAs and NiCr-LDH.

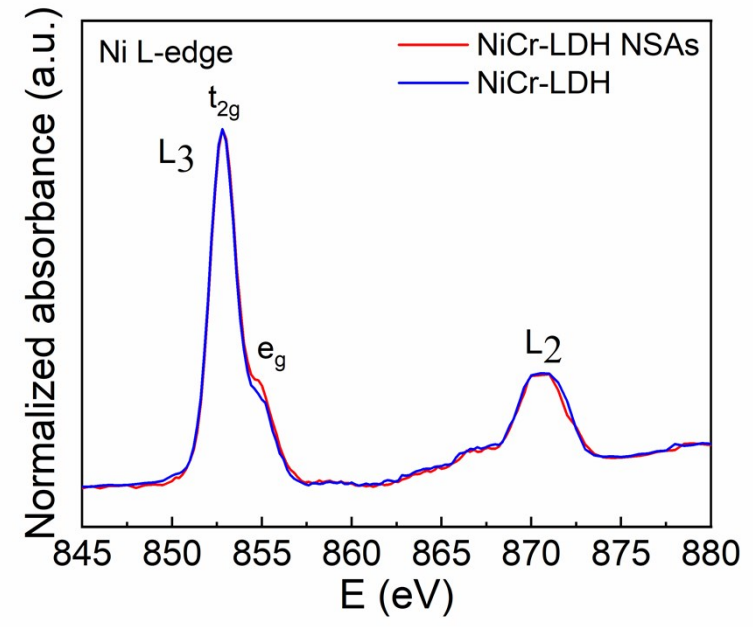

Figure S8. Ni *L*-edge XAS spectra of NiCr-LDH NSAs and NiCr-LDH.

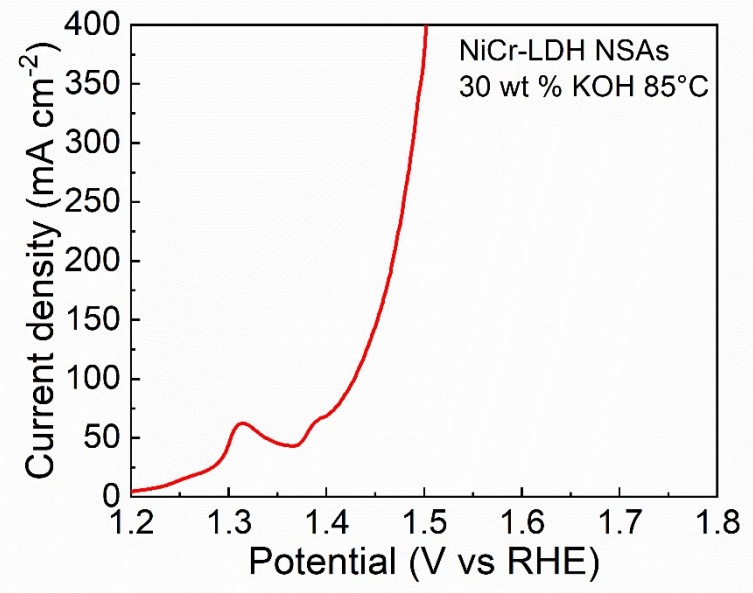

Figure S9. LSV curves of NiCr-LDH NSAs with a constant scan rate of 1 mV s^{-1} for water oxidation in 30 wt % KOH electrolyte at 85 ℃.

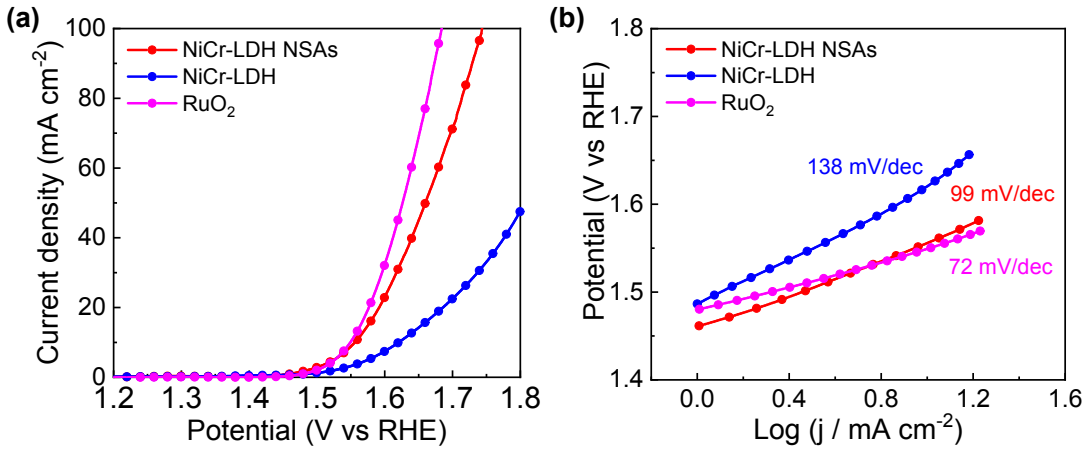

Figure S10. (a) LSV curves, (b) Tafel plots of NiCr-LDH NSAs, NiCr-LDH, and commercial RuO_2 deposited on glassy carbon electrodes.

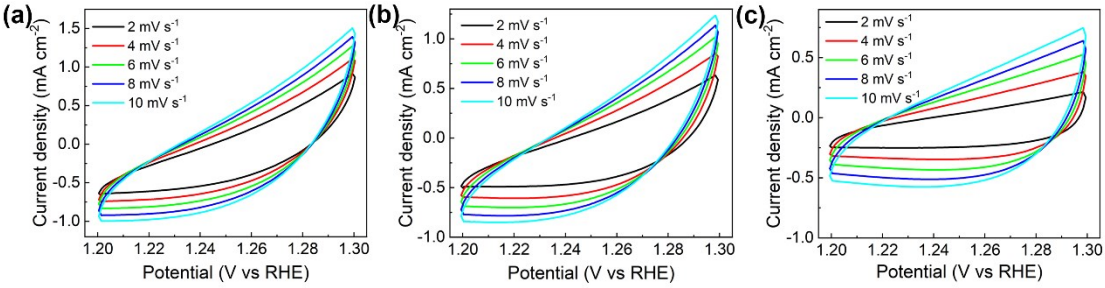

Figure S11. The electric double layer capacitance measurements of (a) NiCr-LDH NSAs, (b) NiCr-LDH and (c) NiCr-LDH NSs powder from 2 to 10 mV/s.

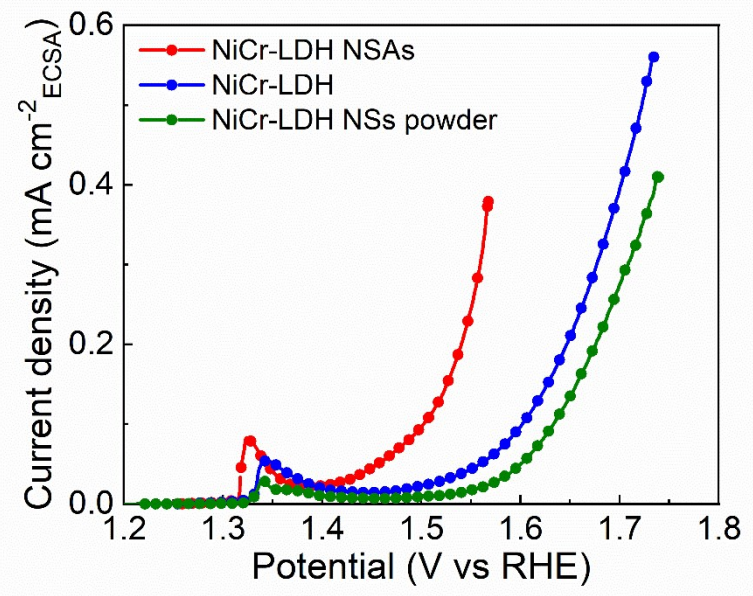

Figure S12. ECSA-normalized LSV curves of different catalysts.

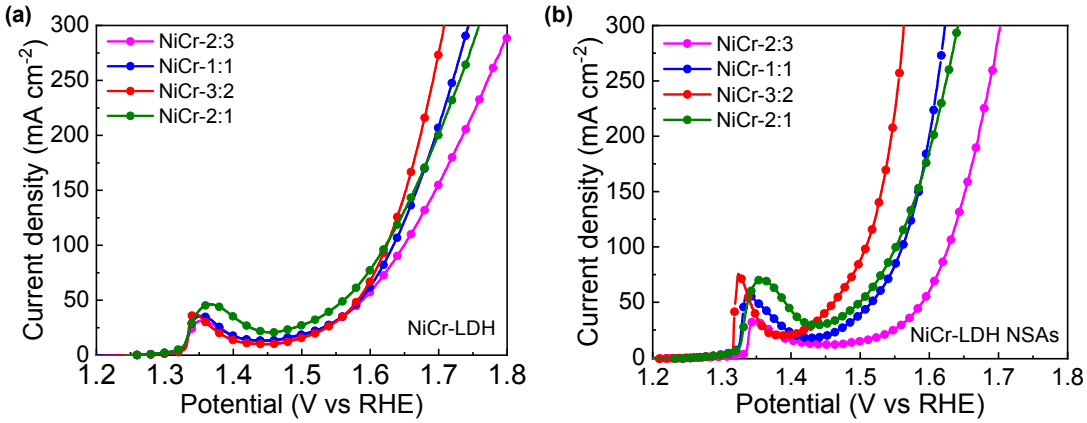

Figure S13. LSV curves of (a) NiCr-LDH and (b) NiCr-LDH NSAs with diffident Ni:Cr ratios.

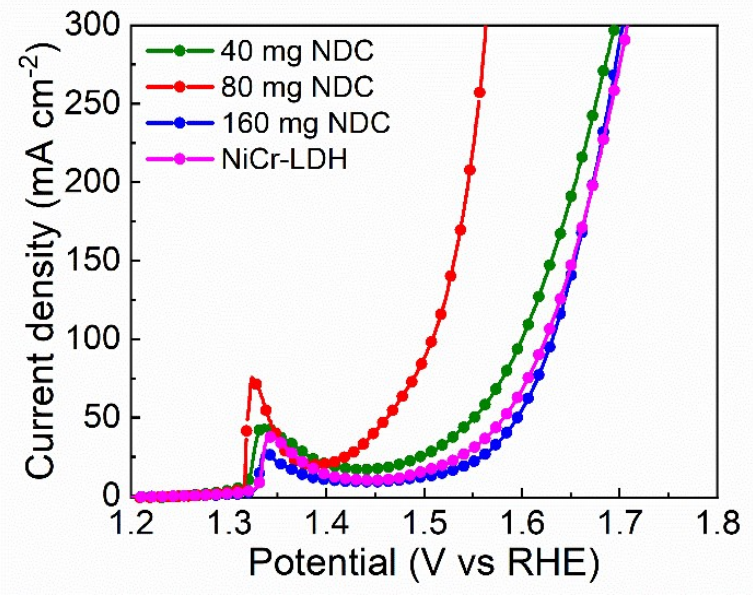

Figure S14. LSV curves of NiCr-LDH NSAs with diffident NDC concentrations.

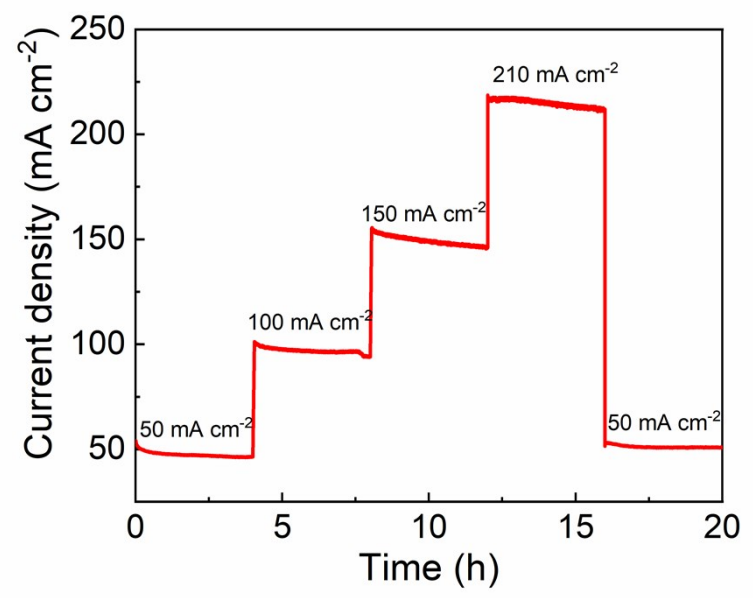

Figure S15. Multi-potential process of NiCr-LDH NSAs.

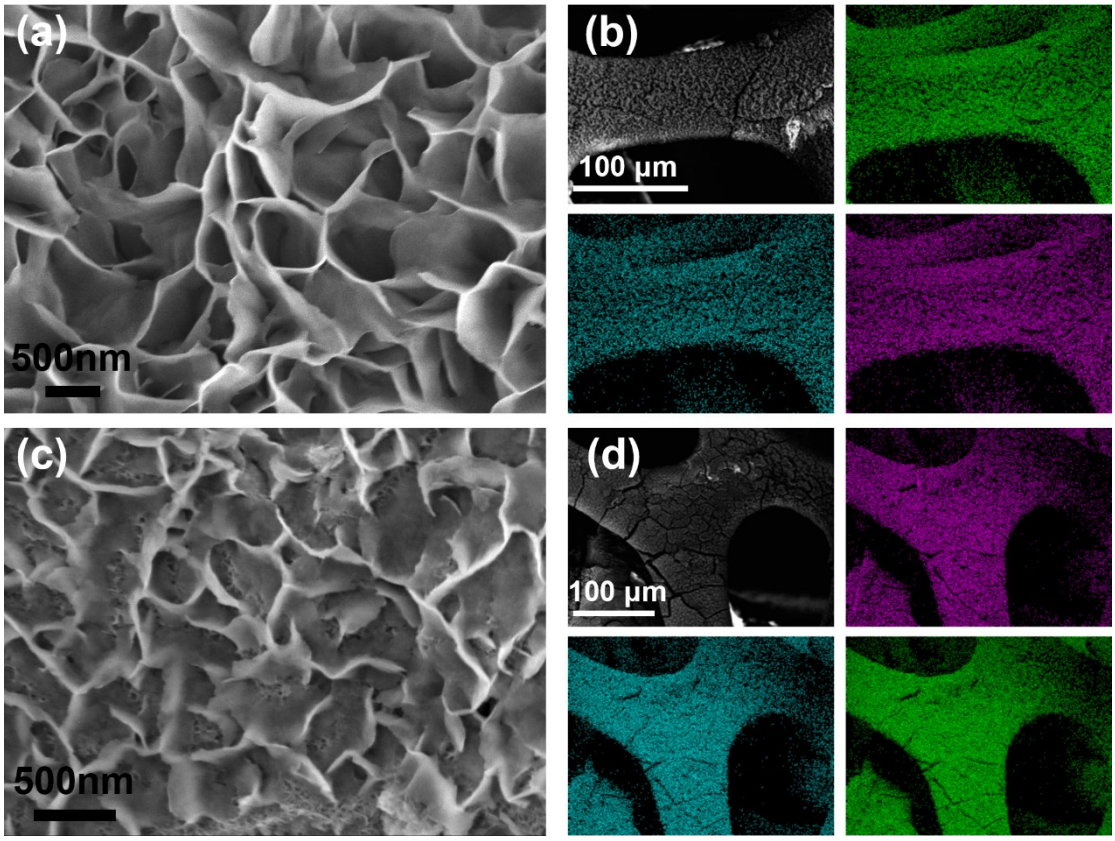

Figure S16. SEM images and EDS mapping images before (a, b) and after (c, d) OER operation for NiCr-LDH NSAs.

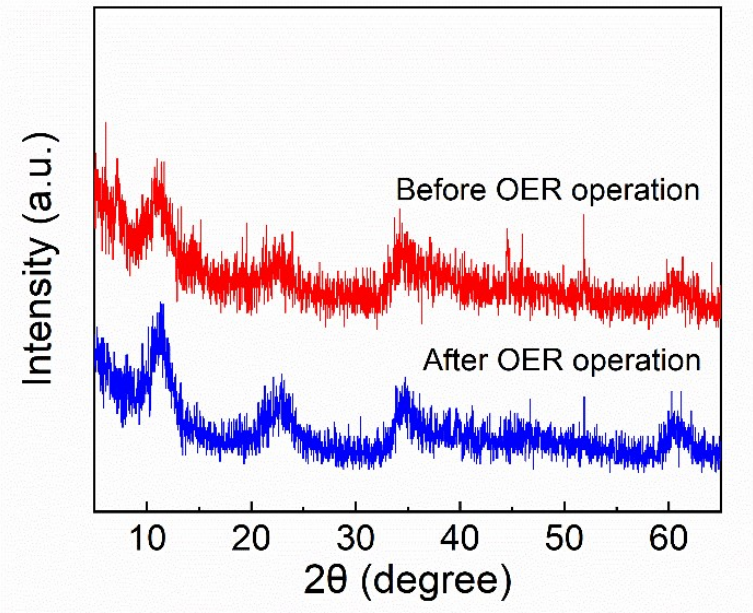

Figure S17. XRD patterns of NiCr-LDH NSAs before and after OER operation.

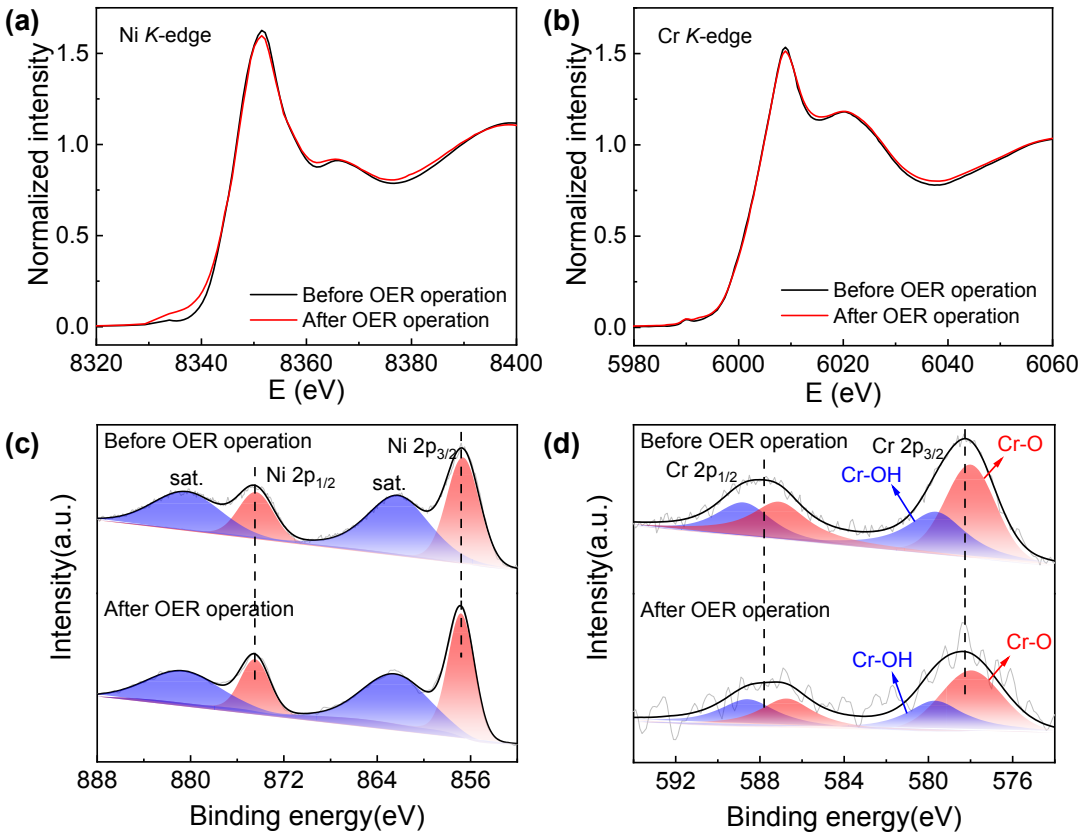

Figure S18. (a) Ni *K*-edge XANES spectra, (b) Cr *K*-edge XANES spectra, (c) high-resolution Ni 2p XPS spectra and (d) high-resolution Cr 2p XPS spectra before and after OER operation for NiCr-LDH NSAs.

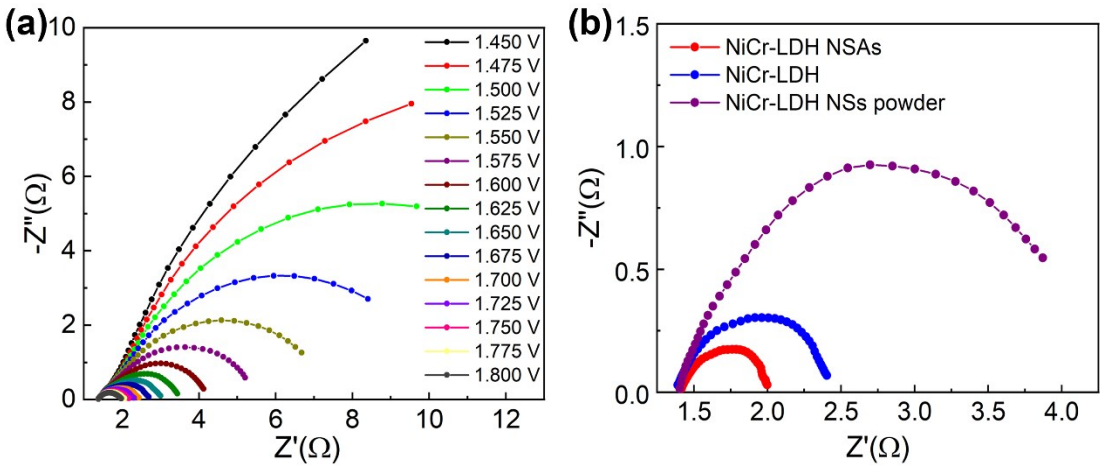

Figure S19. (a) Nyquist plots obtained for NiCr-LDH at different potentials. (b) Nyquist plots of NiCr-LDH NSAs, NiCr-LDH and NiCr-LDH NSs powder at 1.7 V (vs RHE).

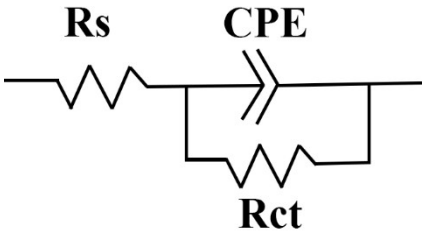

Figure S20. The equivalent circuits of OER.

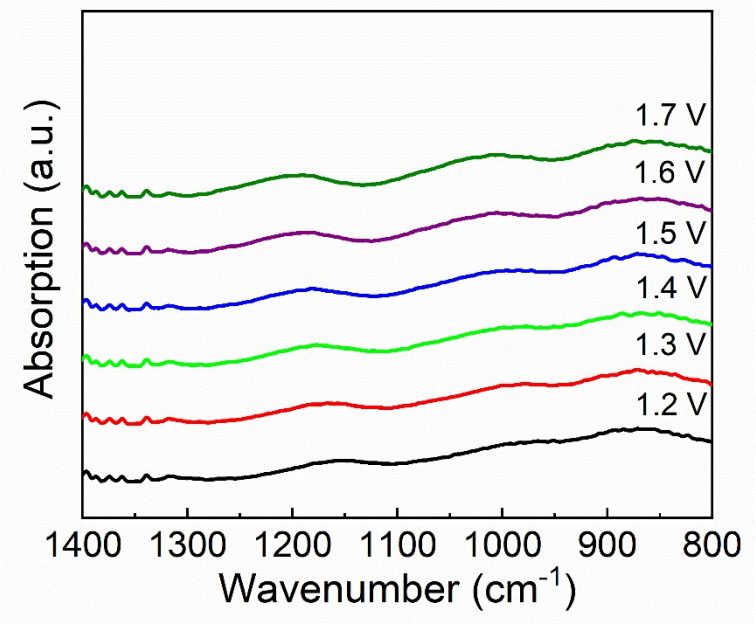

Figure S21. *Operando* SR-FTIR measurements under various potentials for the NiCr-LDH during the OER processes.

Table S1. Local structure parameters of Ni atoms were evaluated by EXAFS analysis.

Samples	Path	*N*	*R* (Å)	$\sigma^2(10^{-3}Å^2)$	ΔE_0 (eV)
NiCr-LDH	Ni-O	5.9	2.05	5.6	-5.48
	Ni-M	5.6	3.11	5.5	-3.25
NiCr-LDH NSAs	Ni-O	5.5	2.05	6.0	-4.25
	Ni-M	5.4	3.11	5.8	-2.95

Table S2. Local structure parameters of Cr atoms were evaluated by EXAFS analysis.

Samples	Path	*N*	*R* (Å)	$\sigma^2(10^{-3}Å^2)$	ΔE_0 (eV)
Pristine NiCr-LDH	Cr-O	5.6	1.98	2.0	0.06
NiCr-LDH NSAs	Cr-O	5.4	1.98	2.1	1.16

Table S3. The EIS fitting data of NiCr-LDH NSAs.

Potential (V vs. RHE)	R_s (Ω)	*CPE* (F)	R_{ct} (Ω)
1.45	1.457	1.312	62.55
1.475	1.44	1.056	10.91
1.5	1.443	0.93095	9.69
1.525	1.44	0.81217	5.459
1.55	1.441	0.74298	3.421
1.575	1.434	0.68703	2.17
1.6	1.437	0.64844	1.675
1.625	1.43	0.60612	1.106
1.65	1.445	0.57598	0.99808
1.675	1.417	0.52144	0.70231
1.7	1.416	0.50127	0.59928
1.725	1.419	0.47614	0.51747
1.75	1.426	0.46597	0.45891
1.775	1.433	0.44807	0.41454
1.8	1.446	0.43435	0.37444

Table S4. The EIS fitting data of NiCr-LDH.

Potential (V vs. RHE)	R_s (Ω)	*CPE* (F)	R_{ct} (Ω)
1.45	1.423	0.58696	86.06
1.475	1.42	0.52123	40.21
1.5	1.413	0.46562	20.12
1.525	1.41	0.42465	11.02
1.55	1.4	0.38767	6.726
1.575	1.395	0.34714	4.429
1.6	1.387	0.3143	3.002
1.625	1.38	0.28789	2.179
1.65	1.385	0.27592	1.664
1.675	1.38	0.25956	1.335
1.7	1.382	0.2759	1.056
1.725	1.368	0.24701	0.93588
1.75	1.369	0.25549	0.78868
1.775	1.366	0.25164	0.69082
1.8	1.37	0.24932	0.60496

Table S5. ICP-MS elemental analysis results of Ni and Cr content for NiCr-LDH and NiCr-LDH NSAs.

Samples	Ni (wt %)	Cr (wt %)	Ni/Cr ratio (at %)
NiCr-LDH	28.91	18.57	1.38
NiCr-LDH NSAs	32.19	19.38	1.47

Table S6. Comparison of OER performance for NiCr-LDH NSAs with other metal-hydroxide-based OER electrocatalysts in 1.0 M KOH (except for special instructions).

Catalysts	Current density (mA cm^{-2})	Overpotential (mV)	Durability	Ref.
NiCr-LDH NSAs	**20**	**182**	**60 h**	**This work**
	100	**279**		
Co-LDH FNSAs	10	300	10000 s	5
Exfoliated CoFe-LDHs/NF	10	237	2000 CV cycles	6
Exfoliated NiCo-LDHs/CFP	10[a]	299	10 h	7
NiFe-LDH/NF	10	182	100 h	8
CoFeCr-LDH/NF	10	202	20 h	4
RuCoV-LDH/NF	20	270	45 h	9
$Ni_{0.83}Fe_{0.17}(OH)_2$	10	245	10 h	10
$Ni/Ni(OH)_2$ NSs/CP	10	270	10 h	11
CoFe@NiFe-LDH/NF	10	190	30 h[b]	12
NiFe-LDH@SWNT	10	250	20 h	13
FeNi LDH/MOF	10	255	24 h	14
^{s}Au/NiFe LDH/Ti mesh	100	270	20 h	15
CoFe-LDH/MXene	10	319	9 h[c]	16
NiFe-LDH/MoS_2	10	250	45000 s	17
FeNi-LDH/CoP/CC	20	231	18.5 h	18
	100	243	N/A	
NiFe LDH@NiCoP/NF	10	340	100 h	19
NiO/NiFe LDH/Cu foam	20	190	10 h	20

MIL-88A/Ni(OH)2-CC	20	280	40 h	[21]
NiCo-LDH/$NiCo_2S_4$/CC	50	254	20 h[d]	[22]

[a] The electrolyte was 1.0 M NaOH. [b] The durability test at a constant current density of 36 mA cm^{-2}. [c] The durability test at a constant current density of 3 mA cm^{-2}. [d] The durability test at a constant current density of 60 mA cm^{-2}.

References

1 W. Zhu, L. Liu, Z. Yue, W. Zhang, X. Yue, J. Wang, S. Yu, L. Wang and J. Wang, *ACS Appl. Mater. Interfaces*, 2017, **9**, 19807-19814.

2 O. Diaz-Morales, I. Ledezma-Yanez, M. T. M. Koper and F. Calle-Vallejo, *ACS Catal.*, 2015, **5**, 5380-5387.

3 W. Ye, X. Fang, X. Chen and D. Yan, *Nanoscale*, 2018, **10**, 19484-19491.

4 Z. Wang, W. Liu, Y. Hu, M. Guan, L. Xu, H. Li, J. Bao and H. Li, *Appl. Catal., B*, 2020, **272**, 118959.

5 T.-J. Wang, X. Liu, Y. Li, F. Li, Z. Deng and Y. Chen, *Nano Res.*, 2019, **13**, 79-85.

6 Y. Wang, Y. Zhang, Z. Liu, C. Xie, S. Feng, D. Liu, M. Shao and S. Wang, *Angew. Chem. Int. Ed.*, 2017, **56**, 5867-5871.

7 Y. Liu, M. Zhang, D. Hu, R. Li, K. Hu and K. Yan, *ACS Applied Energy Materials*, 2019, **2**, 1162-1168.

8 Z. Qiu, C.-W. Tai, G. A. Niklasson and T. Edvinsson, *Energy Environ. Sci.*, 2019, **12**, 572-581.

9 W. Li, B. Feng, L. Yi, J. Li and W. Hu, *ChemSusChem*, 2021, **14**, 730-737.

10 Q. Zhou, Y. Chen, G. Zhao, Y. Lin, Z. Yu, X. Xu, X. Wang, H. K. Liu, W. Sun and S. X. Dou, *ACS Catal.*, 2018, **8**, 5382-5390.

11 L. Dai, Z. N. Chen, L. Li, P. Yin, Z. Liu and H. Zhang, *Adv. Mater.*, 2020, **32**, 1906915.

12 R. Yang, Y. Zhou, Y. Xing, D. Li, D. Jiang, M. Chen, W. Shi and S. Yuan, *Appl. Catal., B*, 2019, **253**, 131-139.

13 H. Liu, J. Zhou, C. Wu, C. Wang, Y. Zhang, D. Liu, Y. Lin, H. Jiang and L. Song, *ACS Sustainable Chem. Eng.*, 2018, **6**, 2911-2915.

14 J. Huo, Y. Wang, L. Yan, Y. Xue, S. Li, M. Hu, Y. Jiang and Q. G. Zhai, *Nanoscale*, 2020, **12**, 14514-14523.

15 J. Zhang, J. Liu, L. Xi, Y. Yu, N. Chen, S. Sun, W. Wang, K. M. Lange and B. Zhang, *J. Am. Chem. Soc.*, 2018, **140**, 3876-3879.

16 C. Hao, Y. Wu, Y. An, B. Cui, J. Lin, X. Li, D. Wang, M. Jiang, Z. Cheng and S. Hu, *Materials Today Energy*, 2019, **12**, 453-462.

17 M. S. Islam, M. Kim, X. Jin, S. M. Oh, N.-S. Lee, H. Kim and S.-J. Hwang, *ACS Energy Lett.*, 2018, **3**, 952-960.

18 K. He, T. Tadesse Tsega, X. Liu, J. Zai, X. H. Li, X. Liu, W. Li, N. Ali and X. Qian, *Angew. Chem. Int. Ed.*, 2019, **58**, 11903-11909.

19 H. Zhang, X. Li, A. Hähnel, V. Naumann, C. Lin, S. Azimi, S. L. Schweizer, A. W. Maijenburg and R. B. Wehrspohn, *Adv. Funct. Mater.*, 2018, **28**, 1706847.

20 Z. W. Gao, J. Y. Liu, X. M. Chen, X. L. Zheng, J. Mao, H. Liu, T. Ma, L. Li, W. C. Wang and X. W. Du, *Adv. Mater.*, 2019, **31**, 1804769.

21 Z. Qian, K. Wang, K. Shi, Z. Fu, Z. Mai, X. Wang, Z. Tang and Y. Tian, *J. Mater. Chem. A*, 2020, **8**, 3311-3321.

22 Y. Liu, Y. Bai, W. Yang, J. Ma and K. Sun, *Electrochim. Acta*, 2021, **367**, 137534.